IEEE Access
Multidisciplinary | Rapid Review | Open Access Journal

Received October 5, 2020, accepted October 27, 2020, date of publication November 2, 2020, date of current version November 11, 2020.

Digital Object Identifier 10.1109/ACCESS.2020.3035235

Soil Moisture Inversion via Semiempirical and Machine Learning Methods With Full-Polarization Radarsat-2 and Polarimetric Target Decomposition Data: A Comparative Study

HÜSEYİN ACAR[1], (Member, IEEE), MEHMET SİRAÇ ÖZERDEM[1], AND EMRULLAH ACAR[2]
[1]Department of Electrical & Electronics Engineering, Faculty of Engineering, Dicle University, 21280 Diyarbakır, Turkey
[2]Department of Electrical & Electronics Engineering, Faculty of Engineering and Architecture, Batman University, 72060 Batman, Turkey

Corresponding author: Hüseyin Acar (hacar@dicle.edu.tr)

This work was supported in part by the research project of The Scientific and Technological Research Council of Turkey (TUBITAK) under Grant 114E543, in part by the Dicle University Scientific Research Projects (DUBAP) Unit, and in part by TARBIL Project.

ABSTRACT In this article, surface soil moisture was retrieved from Radarsat-2 and polarimetric target decomposition data by using semiempirical models and machine learning methods. The semiempirical models and machine learning techniques employed were Oh (1992), Dubois (1995), Oh (2004) and Generalized Regression Neural Network (GRNN), Least Squares – Support Vector Machine (LS-SVM), Extreme Learning Machine (ELM), Kernel based Extreme Learning Machine (KELM), Adaptive Network based Fuzzy Inference System (ANFIS), respectively. In addition, Yamaguchi, van Zyl, Freeman-Durden, H/A/α and Cloude polarimetric target decomposition methods were used in this study. For soil moisture inversion, firstly, preprocessing was applied to the Radarsat-2 image of two different dates with bare and moderately vegetated soil. Then, sigma nought coefficients and the polarimetric decomposition components were extracted as feature vector from preprocessed SAR image pixels corresponding to ground measured points. Lastly, sigma nought coefficients were used in semiempirical inversion models, and sigma nought coefficients and polarimetric decomposition components were used as input to machine learning methods. The best accuracy results for semiempirical models were 13.01 vol. % and 17.91 vol. % Root Mean Square Error (RMSE) for bare and moderately vegetated soil, respectively. The best accuracy for machine learning techniques were 4.04 vol. % and 2.72 vol. % RMSE for two dates, respectively. The results indicated that the machine learning techniques performed much better than the semiempirical models.

INDEX TERMS Machine learning, polarimetric target decompositions, Radarsat-2 imagery, remote sensing, semiempirical models, soil moisture inversion.

I. INTRODUCTION

Soil moisture is a very important parameter for agriculture, hydrology and climatology [1]. Soil moisture in agriculture is closely related to plant growth. Accurate and reliable measurement of soil moisture is useful in prevention of wasteful use of water resources and soil management [2].

Ground measurement methods used to determine soil moisture have many disadvantages in terms of time, cost and labor. Therefore, a great number of researches have been done by using remote sensing technologies, especially with active microwave sensors, in recent years in order to retrieve soil moisture because radar return is sensitive to changes in soil moisture content on the surface [3]. Synthetic Aperture Radar (SAR) sensor which is an active microwave sensor is important in agricultural monitoring in such working areas as yield forecasting, mapping and soil moisture retrieving [4]. Since the Radarsat-2 satellite has an active SAR sensor, it does not need sunlight and because it operates at a longer wavelength than optical sensor satellites, it can measure in adverse weather conditions (cloudy, rainy and foggy weather) and is not very sensitive to atmospheric effects. Radarsat-2 uses the C-band microwave frequencies of the electromagnetic spectrum and operating frequency is 5.405 GHz

The associate editor coordinating the review of this manuscript and approving it for publication was Hao Ji.

and wavelength is 5.5 cm. The sensor is fully polarimetric (captures both amplitude and relative phase of returned signal in all polarizations: HH, VV, HV, VH), where the first letter represents the transmitted horizontal (H) or vertical (V) polarization and the second letter indicates the received polarization) [5]. The most important sensor parameters that affect radar backscattering are incidence angle, wavelength and polarization of the sensor, while the important target parameters are surface roughness, surface dielectric coefficient and vegetation. Dielectric property describes the ability of a wave to propagate through a material. Dielectric properties of soil are closely related to moisture content and are the second most important factor that controls backscattering.

Full polarimetric SAR data provides information by multiple polarizations with very high spatial and temporal resolutions and penetrates the vegetative canopies [6] and contains the contributions of soil and vegetated fields, while vegetation contributions change with phenological stages of the plant. To estimate the soil moisture over vegetated areas accurately, the backscattering contributions by vegetation and ground must be separated from the total measured backscattering [7].

The approaches used to achieve soil moisture inversion can be grouped into two categories: The first group includes empirical, semiempirical and physical models, while the second includes machine learning based approaches. Empirical models establish regression equations between backscatter and volumetric soil moisture as collected in field sampling. For bare or barely vegetated soils, backscatter is a function of RMS height (roughness) and volumetric soil moisture. For vegetated surfaces, backscatter contributions from the vegetation canopy and from ground-canopy interactions are added. Semiempirical models establish the relations between backscatter (or backscatter ratios) and relative dielectric permittivity. The most widely used semiempirical models are the Oh (1992) [8], Dubois (1995) [9] and Oh (2004) [10] models. All three models are valid through L, C and X bands. The most widely used physical model for soil moisture retrieval is the integral equation model [11]. Due to its complex formulation, it is commonly applied by running a number of forward iterations with a range of roughness and dielectric characteristics to populate lookup tables rather than inverting the model to estimate soil moisture. The main difficulty with physical models lies in finding closed solutions for their inversion. Machine learning approaches used to retrieve soil moisture include Artificial Neural Networks (ANN), Support Vector Machine (SVM), Relevant Vector Machine (RVM) and Adaptive Network Based Fuzzy Inference System (ANFIS) [12]. These approaches were originally developed to solve classification problems but were successfully applied to inversion problems later. The advantages of these approaches are that they are generally flexible and can be used for any learning task, while their disadvantage is requiring large ground truth measurements.

In the literature, many studies have been conducted to retrieve soil moisture. For example, Satalino *et al.* utilized an ANN model to retrieve soil moisture from ERS dataset [13]. The training dataset was obtained from the simulated data of IEM model. The performance of this approach was measured with 6% RMSE value for estimated volumetric soil moisture content. In another study [14], different configurations of ANN were used to estimate soil moisture content form ASAR and Radarsat-2 data. The accuracy was presented as 5% RMSE value. Pasolli *et al.* employed an SVR model on Radarsat-2 imagery [15]. They used HH and HV channels of polarimetric features to inverse the soil moisture and the accuracy was presented with an RMSE of 4.85%.

This article evaluates semiempirical models and different machine learning methods for soil moisture inversion. The contributions of this study are using different machine learning models and different polarimetric coefficients feature vector as model inputs. The proposed approach in this study has never been investigated using agricultural areas in Turkey. As far as is known, Yamaguchi decomposition coefficients are used to estimate the soil moisture for the first time.

The following sections are organized as follows: In the second section, study area, ground measurements, properties and preprocessing of Radarsat-2 imagery are presented. In the third section, the formulations of semiempirical and machine learning methods and polarimetric decomposition models are given. In the following sections, study results, discussion and conclusions are presented.

II. MATERIALS

A. STUDY AREA

The study area selected is located within the agricultural fields of Dicle University in Diyarbakir province in the southeast of Turkey (40°04′ −40°26′E, 37°46′ −38°04′N) and consists of two parts of a total of 22 km^2. The average height of study area is 650 m. Average rainfall in March and June is 65 mm and 8 mm, respectively, and average temperature is 8 and 26 °C, respectively. Wheat and corn are mostly cultivated in these agricultural fields. The map showing the study area is given in Figure 1.

B. GROUND MEASUREMENTS

Detailed information on collecting samples is given in [16], but can also be briefly mentioned here. The ground measurements were conducted on 10 June 2015 and 3 March 2016 simultaneously with the Radarsat-2 data acquisition. Firstly, the study area was divided into areas of 100 m × 100 m and at least one soil sample was taken from each area. The distance between ground measurements is approximately 100 m and soil samples were taken with 3-5 cm depth. Soil samples were filled in 100 cm^3 metal cylinders. The location information of these samples was recorded with the help of GPS device. Soil moisture content was measured by gravimetric methods at Dicle University research labs. The number of soil samples taken from the study area on 10 June 2015 and 3 March 2016 is 272 and 156, respectively. Other information on soil moisture measurements performed on these dates is presented in Table 1.

TABLE 1. Soil moisture measurements (%).

Measurement date	Study area	Number of samples	Min	Max	Mean	Standard deviation
10 June 2015	Bare	272	0.79	44.73	7.46	7.01
3 March 2016	Moderately Vegetated	156	25.38	43.20	34.45	2.89

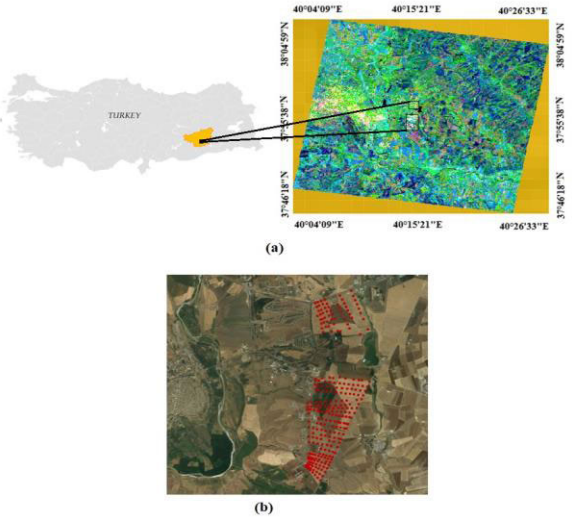

FIGURE 1. The map of study area (a) two sites of study area are marked with black rectangles on Freeman-Durden decomposition RGB image where red is for double bounce, green is for volume and blue is for surface scattering components, (b) sample points are shown in red on the Google Earth image.

TABLE 2. Information of the acquired Radarsat-2 IMAGERY.

Date of acquisition	Orbit direction	Beam model	Incidence angle
10 June 2015	Descending	Q29	46.8° – 48°
3 March 2016	Descending	Q13	32.39° – 34.04°

C. SAR IMAGERY AND PREPROCESSING

Radarsat-2 is a spaceborne radar satellite launched by the Canadian Space Agency in 2007 and has C-band microwave sensors. To estimate soil moisture, two full polarimetric single-look complex (SLC) products were utilized in this study. Information of the acquired Radarsat-2 imagery was given in Table 2.

The SNAP Sentinel-1 toolbox was used for preprocessing of SAR products. Preprocessing steps were radiometric calibration, speckle filtering and terrain correction. Firstly, radiometric calibration was applied to provide imagery in which the pixel values could be directly related to radar backscatter of the scene. Then, speckle filtering step was applied by the refined Lee filter with 7×7 sliding window to remove speckle noise. The resolution of the speckle filtered image is 4256×6149 pixels. Lastly, terrain correction was achieved using SRTM-3 Digital Elevation Model (DEM) and WGS84 map projection. The resolution of terrain corrected image is 6226×5171 pixels. The spatial resolution of the final image is 6.43 m. As a result of these steps, the sigma nought radar scattering coefficients were obtained from SAR data. In addition to these steps, the T3 coherency matrix was obtained before the terrain correction step. This step is required to obtain polarimetric target decomposition components. Sample Radarsat-2 images whose pre-processes are completed are presented in Figure 2.

III. METHODS

A. SEMIEMPIRICAL MODELS

1) OH MODELS

Oh (1992) [8] and Oh (2004) [10] proposed semiempirical backscatter models for bare soil surfaces by using the theoretical model, backscatter and SAR measurements. The models define co-polarization ratio (p) and cross polarization ratio (q) depending on incidence angle (θ), wave number (k), standard deviation of the surface height (s), and volumetric soil moisture (m_v). Oh *et al.* (1992) presented the model firstly as shown in equations (1) and (2). The model is for bare soils and is valid for $0.1 \leq ks \leq 2.5$, $0.09 \leq m_v \leq 0.31$ and $10° \leq \theta \leq 70°$.

$$p = \sigma^0_{HH}/\sigma^0_{VV} = [1 - (\frac{2\theta}{\pi})^{1/(3\Gamma_0)}.e^{-ks}]^2 \quad (1)$$

$$q = \sigma^0_{HV}/\sigma^0_{VV} = 0.23\sqrt{\Gamma_0}[1 - e^{-ks}] \quad (2)$$

$$\Gamma_0 = \left|\frac{1 - \sqrt{\varepsilon_r}}{1 + \sqrt{\varepsilon_r}}\right|^2 \quad (3)$$

Soil moisture estimation using the Oh (1992) model from the remotely sensed image, the backscattering coefficients (σ^0_{HH}, σ^0_{HV} and σ^0_{VV}), θ and wavelength (λ) must be known. If the p and q equations are arranged in a manner that the term e^{-ks} is eliminated, then the equation (4) is obtained. When this equation is solved iteratively for Γ_0 (Fresnel reflection), the dielectric constant can be calculated from equation (3), and then the volumetric soil moisture can be obtained with the polynomial (5) proposed in [17].

$$\left(\frac{2\theta}{\pi}\right)^{1/3\Gamma_0} \cdot \left[1 - \frac{q}{0.23\sqrt{\Gamma_0}}\right] + \sqrt{p} - 1 = 0 \quad (4)$$

$$m_v = -5.3 + 2.92(\varepsilon'_r) + 0.055(\varepsilon'_r)^2 + 0.0043(\varepsilon'_r)^3 \quad (5)$$

Equations (6) and (7) were modified, and a new equation (given in (8)) for the cross-polarized backscatter coefficient was presented in [18]. Considering that the measurement of the correlation length is not precise [19] and the ratio of q is insensitive to the roughness parameter, Oh proposed in [10] a new equation for q in neglecting the correlation length. The model is for bare soils and is valid for $0.13 \leq ks \leq 6.98$, $0.04 \leq m_v \leq 0.291$ and $10° \leq \theta \leq 70°$.

$$p = 1 - (\frac{\theta}{90^0})^{0.35.m_v^{-0.65}} e^{-0.4(ks)^{1.4}} \quad (6)$$

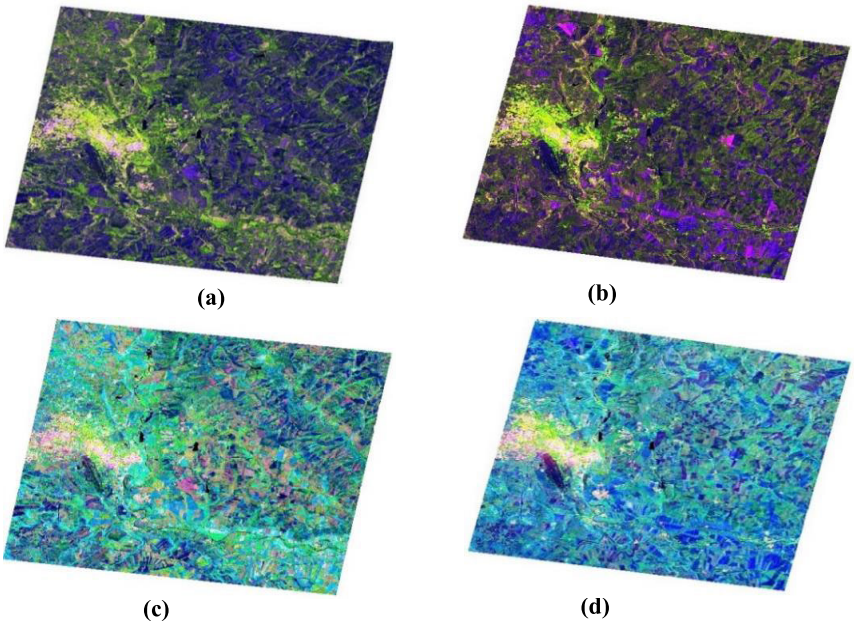

FIGURE 2. RGB images derived from preprocessed full scene Radarsat-2 data (a) 10 June 2015 and (b) 3 March 2016 where red is for HH polarization, green is for HV polarization, blue is for HH/HV, (c) 10 June 2015 and (d) 3 March 2016 where is red for double bounce, green is for volume and blue is for surface scattering components of Yamaguchi decomposition.

$$q = 0.095(0.13 + \sin 1.5\theta)^{1.4}(1 - e^{-1.3(ks)^{0.9}}) \quad (7)$$

$$\sigma^0_{VH} = 0.11 m_v^{0.7} \cos^{2.2}\theta(1 - e^{-0.32(ks)^{1.8}}) \quad (8)$$

An inversion model was created from the Oh (2004) model to estimate soil moisture. For this purpose, equation (8) is arranged for ks as follows:

$$ks = \left[-3.125 In\left(\frac{\sigma^0_{VH}}{0.11 m_v^{0.7}(\cos\theta)^{2.2}}\right)\right]^{5/9} \quad (9)$$

Equation (9) is substituted in equation (7) and a non-linear equation (10) is obtained for m_v. This equation is solved for the initial value $m_v = 0.5$ by iterative numerical methods.

$$1 - \left(\frac{\theta}{90^\circ}\right)^{0.35 m_v^{-0.65}} \cdot \exp\left(-0.4\left\{\left[-3.125 In\left(\frac{\sigma^0_{VH}}{0.11 m_v^{0.7}(\cos\theta)^{2.2}}\right)\right]^{5/9}\right\}^{1.4}\right) - p = 0 \quad (10)$$

The first estimation of ks is obtained by substituting m_v's first estimation in equation (9). The second estimation of ks is derived from equation (7):

$$ks = \left[In\left(1 - \frac{q}{0.095(0.13\sin(1.5\theta))^{1.4}}\right) / -1.3\right]^{10/9} \quad (11)$$

Using this second estimate of ks, two more estimations of m_v are derived from equations (6) and (8):

$$m_v = \left[\frac{\sigma^0_{VH}}{0.11(\cos\theta)^{2.2}[1 - \exp(-0.32(ks)^{1.8}]}\right]^{10/9} \quad (12)$$

$$m_v = \left[In\left(\frac{1-p}{\exp(-0.4(ks)^{1.4}/0.35 In\theta}\right)\right]^{-20/13} \quad (13)$$

This process ends with two estimates of s and three estimates of m_v. s and m_v's weighted averages are obtained with equations (14) and (15).

$$s = \frac{s_1 * w_1 + s_2 * 0.25 w_2}{w_1 + 0.25 w_2} \quad (14)$$

$$m_v = \frac{m_{v1} * w_3 + m_{v2} * w_4 + m_{v3} * w_5}{w_3 + w_4 + w_5} \quad (15)$$

At the final stage, it is confirmed whether the estimates produced are within the model validity ranges. Due to the averaging process in the previous stage, estimates are likely to be outside the model validity ranges.

2) DUBOIS MODEL

Dubois *et al.* [9] proposed a semiempirical approach to model σ^0_{HH} and σ^0_{VV} radar backscatter coefficients. σ^0_{HH} and σ^0_{VV} are expressed by the incidence angle, dielectric coefficient, standard deviation of the surface height and wavelength. The model is for bare soils and is valid for $k.s \leq 2.5$, $m_v \leq \%35$ and $\theta \geq 30^\circ$.

$$\sigma^0_{HH} = 10^{-2.75}\left(\frac{\cos^{1.5}\theta}{\sin^5\theta}\right)10^{0.028.\varepsilon_r.\tan\theta}(k.s.\sin\theta)^{1.4}\lambda^{0.7} \quad (16)$$

$$\sigma^0_{VV} = 10^{-2.35}\left(\frac{\cos^3\theta}{\sin^3\theta}\right)10^{0.046.\varepsilon_r.\tan\theta}(k.s.\sin\theta)^{1.1}\lambda^{0.7} \quad (17)$$

For the Dubois (1995) inversion model, it is solved for $\varepsilon_r \tan\theta$ one of the equations given in (16) and (17) and substituted in the other equation. The resulting equation is solved to obtain surface roughness (ks). The obtained ks is substituted by the equation (16) and the dielectric constant is estimated.

$$\varepsilon' = \frac{\log_{10}(\sigma^0_{HH})10^{2.75}(\cos\theta)^{-1.5}(\sin\theta)^5(k.s.\sin\theta)^{-1.4}\lambda^{-0.7}}{0.028\tan\theta} \quad (18)$$

Finally, the dielectric constant estimation is converted to volumetric soil moisture estimation by using empirically derived 3rd order polynomial (5).

B. MACHINE LEARNING METHODS

1) LEAST SQUARE – SUPPORT VECTOR MACHINES (LS-SVM)

Vapnik proposed the Support Vector Machines (SVM) method based on machine learning theory and quadratic programming solution in order to minimize the disadvantages of Artificial Neural Networks [20]. A support vector machine optimally creates a hyper plane that divides the data into two categories. In SVM regression, an approach error is used instead of a margin between the most appropriate separating hyper plane and support vectors [21].

Suykens *et al.* proposed using the Least Squares - Support Vector Machines (LS-SVM) to simplify conventional SVM [22]. LS-SVM has been used for classification in various areas of pattern recognition and has recently addressed regression problems successfully. LS-SVM has similar advantages as SVM, but its additional advantage is that it requires solving a series of linear equations that are much easier and simpler in calculation.

In this method, the error optimization problem is provided with the equation (19) using the $\{x_i, y_i\}$ training data set presented to the model [23]. LS-SVM for regression is formulated

$$\min J(w, \xi) = \frac{1}{2}\|w\|^2 + \frac{C}{2}\sum_{i=1}^{n}\xi_i^2$$
$$y_i = \langle w, \varphi(x_i)\rangle + b + \xi_i, \quad i = 1, \ldots, N \tag{19}$$

where $\xi_i \in R$ are error variables, w are weights, $\varphi(x_i)$ is the kernel function that allows input space to be mapped non-linearly to a multi-dimensional feature space, b is bias and $C \geq 0$ is a regularization constant.

The solution of the optimization problem in LS-SVM is realized by taking into account Lagrange multipliers. Lagrangian is given by

$$L_{LS-SVM} = \frac{1}{2}\|w\|^2 + \frac{1}{2}C\sum_{i=1}^{N}\xi_i^2 - \sum_{i=1}^{N}\alpha_k \times \{\langle w, \varphi(x_i)\rangle + b + \xi_i - y_i\} \tag{20}$$

with Lagrange multipliers $\alpha_k \in R$. While these multipliers must be positive in the standard SVM method, they can also be negative values in the LS-SVM method. The function estimation for the LS-SVM model is arranged as in Equation 21, after eliminating w and the error term by applying the first order partial derivatives in Equation 20.

$$\widehat{y}_i = \sum_{i=1}^{N}\alpha_k K(x_i, x) + b \tag{21}$$

Here, the $K(x_i, x)$ function refers to the kernel function.

2) GENERALIZED REGRESSION NEURAL NETWORK (GRNN)

GRNN is a radial-based feedforward ANN model proposed by Donald Specht in 1991 [24], and unlike the back-propagation method, it does not require an iterative training process. GRNN consists of four layers, each associated with the next layer: input layer, pattern layer, summation layer and output layer.

GRNN is a probabilistic neural network containing the probability distribution function. The training data set consists of input x corresponding to each y output of the GRNN regression model.

$$E[(y|x)] = \frac{\int_{-\infty}^{\infty} yf(x, y)dy}{\int_{-\infty}^{\infty} f(x, y)dy} \tag{22}$$

where $E[(y|x)]$ is the expected value of the output y given input vector x and $f(x, y)$ is the probability density function of x and y. The estimated y can be computed as:

$$\hat{y}(x) = \frac{\sum_{i=1}^{n} y^i \exp\left(-\frac{C_i}{\varsigma}\right)}{\sum_{i=1}^{n}\exp\left(-\frac{C_i}{\varsigma}\right)}, \quad C_i = \sum_{j=1}^{p}\left|x_j - x_j^i\right| \tag{23}$$

where n is number of training samples, ς is spread parameter and C_i is the squared distance between input vector x and training vector x^i.

3) EXTREME LEARNING MACHINE (ELM) AND KERNEL ELM (KELM)

ELM is a simple, fast and robust learning method, recommended in [25] and developed for Single Hidden Layer Feed Forward Neural Networks. While the input layer weights and bias values are randomly selected in the ELM, the output layer weights are calculated analytically. In this way, the learning process is extremely accelerated.

The input of the output layer for any transfer function $(g(\cdot))$ of an ANN is

$$H = \begin{pmatrix} g(w_{1,1}x_1 + b_1) & \cdots & g(w_{1,m}x_m + b_m) \\ \vdots & \ddots & \vdots \\ g(w_{n,1}x_n + b_1) & \cdots & g(w_{n,m}x_m + b_m) \end{pmatrix} \tag{24}$$

where n is input neuron number, m is hidden layer neuron number, $w_{i,j}$ are input layer weights and b_j are bias values.

$$y = H\beta \tag{25}$$

is output equation of ANN and β indicates output weights. The output weights are calculated by equation (26).

$$\widehat{\beta} = H^{+}y \tag{26}$$

where H^{+}, the inverse of H matrix is calculated by generalized inverse Moore-Penrose matrix.

By including a kernel function in ELM, errors in weights can be reduced and the system's robustness and generalization ability can be increased. The weights in the Kernel ELM are calculated as follows:

$$\beta = \left(\frac{I}{C} + K\right)^{-1}y \tag{27}$$

where C represents regularization coefficient and K is kernel.

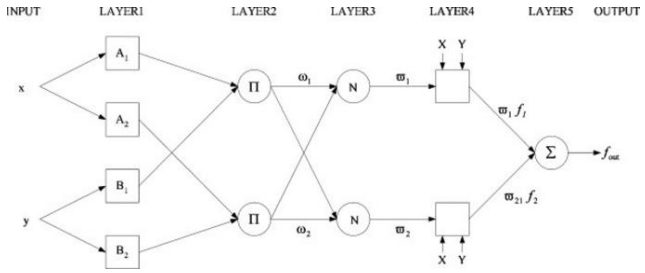

FIGURE 3. ANFIS architecture.

4) ADAPTIVE NETWORK BASED FUZZY INFERENCE SYSTEM (ANFIS)

ANFIS is a multi-layered adaptive network that combines the learning ability of artificial neural networks and the inference principles of fuzzy logic and was originally presented in [26]. This hybrid learning algorithm uses both back propagation and least square algorithms. In order to apply the ANFIS method, first of all, a data set containing inputs and outputs is required. Then, the number and type of membership functions are selected, and the model established accordingly is created using a learning algorithm. The method uses the created fuzzy set of if-then rules. ANFIS architecture is created by determining parameters to minimize the difference between output and target values.

Five layers are necessary to create the ANFIS inference system. Each of these layers consists of several nodes defined by the node functions. The ANFIS architecture is given in Figure 3, while the adjustable parameters are denoted with square nodes, the nodes which parameters are fix are denoted in circles.

C. POLARIMETRIC DECOMPOSITION MODELS

Polarimetric decomposition is mainly based on the scattering matrix explaining how radar targets or ground surface objects distribute electromagnetic energy. The main purpose of target decomposition methods is to decompose measured polarimetric matrix into a summation of a set of basic scattering mechanisms, and each scattering mechanism corresponds to a physical mechanism and the dominant scattering mechanism can be determined. Hence, the polarimetric target decomposition methods simplify the interpretation of the scattering process.

Decomposition theorems are divided into two as coherent and incoherent target decompositions. The incoherent decompositions give better results due to the targets distributed heterogeneously and are more common on the surface of the earth. Polarimetric decomposition can be classified as follows: coherent decomposition based on the S scattering matrix (Pauli, Touzi, Cameron decompositions), model-based decomposition of the coherent (T3) and covariance (C3) matrices (Yamaguchi, Freeman-Durden decompositions), and coherent (T3) and covariance (C3) decomposition based on the eigenvalue or eigenvector (H / A / Alfa, van Zyl, Cloude decompositions). Model-based decomposition has merits of interpreting scattering mechanisms directly relating to physical structures with canonical physical models.

TABLE 3. Polarimetric decomposition methods and their components.

Polarimetric decomposition	Components
Freeman Durden	Surface scattering, Double bounce scattering, Volume scattering
Yamaguchi	Surface scattering, Double bounce scattering, Volume scattering and Helix scattering
van Zyl	Surface scattering, Double bounce scattering, Volume scattering
Cloude-Pottier (H/A/α)	Entropy, Anisotropy, Alpha angle
Cloude	Surface scattering, Double bounce scattering, Volume scattering

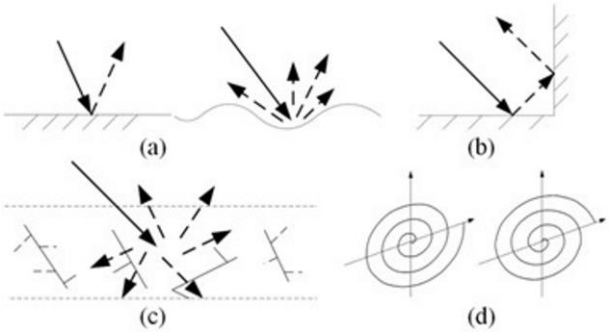

FIGURE 4. Scattering mechanisms (a) Surface scattering, (b) Double bounce scattering, (c) Volume scattering and (d) Helix scattering.

Polarimetric decomposition models and their components used in this study are shown in Table 3 and scattering mechanisms are shown in Figure 4.

Freeman-Durden is one of the first three-component incoherent model-based decompositions. The three-component scattering mechanism includes surface scattering from a rough surface, double bounce scattering from the dihedral surface, and volume scattering from randomly directed dipoles. Freeman-Durden decomposition assumes the reflection symmetry condition for which the cross-correlation and co-polarization are always zero. Freeman-Durden decomposition provides a more realistic representation as it uses scattering patterns with dielectric surface [27].

Based on the three-component scattering model approach, Yamaguchi *et al.* proposed a four-component scattering model [28], introducing a helix scattering term. Helix scattering model removes the reflection symmetry assumption since it is not always valid for various land covers except for man-made structures and complex-shaped targets. Freeman-Durden and Yamaguchi decompositions have advantages such as simplicity, easy physical interpretation, computational efficiency and relatively good performance. However, volume scattering contribution is overestimated because the dynamic ranges of commonly used volume scattering models are very limited.

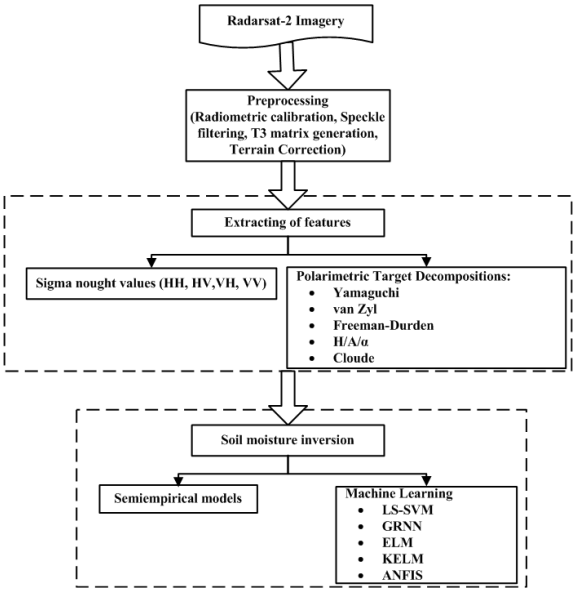

FIGURE 5. Flow chart of study.

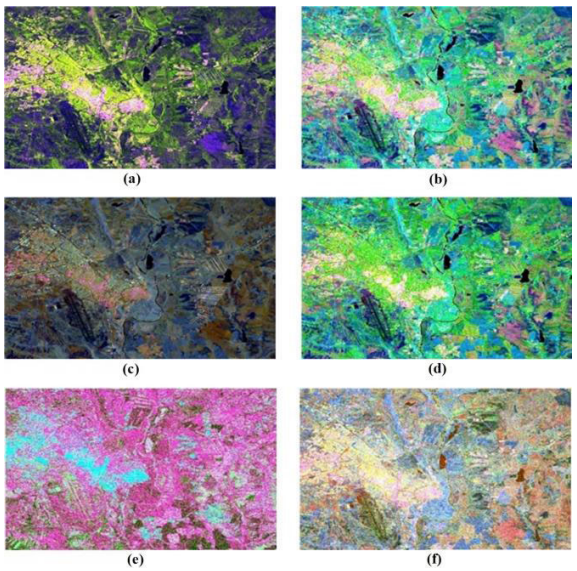

FIGURE 6. The preprocessed Radarsat-2 SAR data scene which includes study area derived for 10 June 2015 using (a) sigma nought tecnique, (b) Yamaguchi, (c) van Zyl, (d) Freeman-Durden, (e) H/A/α and (f) Cloude decomposition models.

Van Zyl decomposition is an eigenvector-based decomposition method [29], and the main idea of this decomposition is to avoid the occurrence of nonphysical negative power. In Freeman-Durden and Yamaguchi decompositions, negative eigenvalues of covariance matrix can be generated for surface and double-bounce scattering components. Thus, the results of these decompositions are physically incorrect. The polarimetric components of van Zyl decomposition are surface scattering, double bounce scattering and volume scattering.

Cloude decomposition is an eigenvector-based decomposition that is based on an algorithm to identify the dominant scattering mechanism to extract the largest eigenvalue of coherency matrix [30]. The components of this

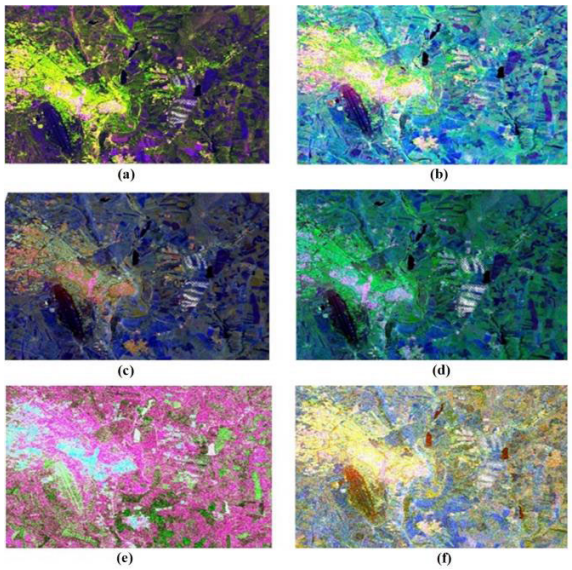

FIGURE 7. The preprocessed Radarsat-2 SAR data scene which includes study area derived for 3 March 3016 using (a) sigma nought tecnique, (b) Yamaguchi, (c) van Zyl, (d) Freeman-Durden, (e) H/A/α and (f) Cloude decomposition models.

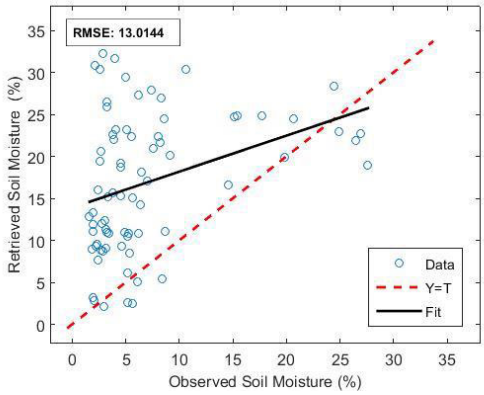

FIGURE 8. Soil moisture inversion using semiempirical models for 10 June 2015 Radarsat-2 data with Dubois (1995) model.

decomposition are surface scattering, double bounce scattering, and volume scattering.

Cloude-Pottier decomposition is based on eigenvector decomposition of the coherency matrix and is also called as H / A / α decomposition. This method decomposes complex scattering into three polarimetric parameters, which are entropy (H), anisotropy (A), and mean alpha angle (α). Low entropy values generally define the dominant scattering mechanisms, and high entropy values define the random combinations of different scattering mechanisms [31]. The alpha angle has three specific states as $\alpha = 0°$, $45°$ and $90°$ due to surface scattering, volume scattering and double-bounce scattering, respectively. Anisotropy is a useful parameter to distinguish scattering mechanisms and define the relative importance of second and third eigenvalues.

In this study, the sigma nought radar backscatter coefficients and the components of Yamaguchi, van Zyl, Freeman Durden, H / A /α and Cloude polarimetric target decompositions were extracted as feature vectors from the preprocessed Radarsat-2 images of 10 June 2015 and 3 March 2016 for

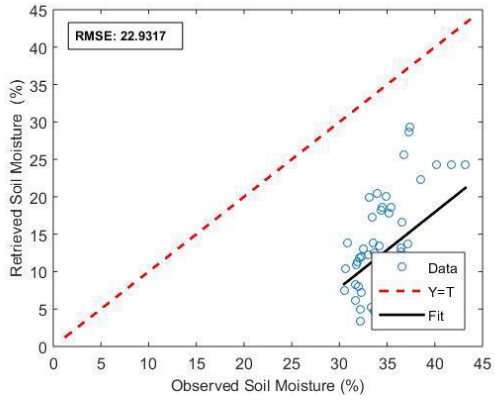

FIGURE 9. Soil moisture inversion using semiempirical models for 3 March 2016 Radarsat-2 data with Oh (1992) model.

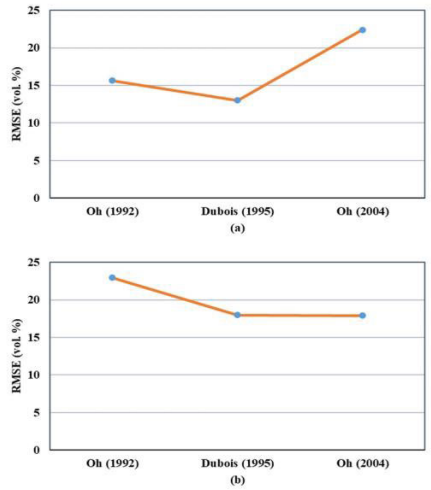

FIGURE 10. Soil moisture inversion using semiempirical models (a) 10 June 2015 Radarsat-2 data, (b) 3 March 2016 Radarsat-2 data.

the inversion of soil moisture using the semiempirical and machine learning models. While the radar backscatter coefficients ($\sigma^o_{HH}, \sigma^o_{HV}, \sigma^o_{VH}, \sigma^o_{VV}$) were used for retrieving with the semiempirical models, the polarimetric decomposition components and the radar backscatter coefficients were utilized as the input of the machine learning models for inversion process. The flow chart of the study is given in Figure 5.

IV. RESULTS AND DISCUSSION

In this section, the results of soil moisture inversion from Radarsat-2 images are presented. The semiempirical and machine learning models employed for this purpose and analyzes for two different periods are given.

To obtain the sigma nought values and polarimetric decomposition parameters to be used in the inversion of soil moisture from Radarsat-2 SAR data, firstly, the raw Radarsat-2 image was preprocessed. The preprocessing steps applied to the images were detailed in the section SAR Imagery and Preprocessing. The GPS data corresponding to the points of the ground measurements were processed on the preprocessed image. After that, a cell consisting of 3×3 pixels of the image around ground measurement point were averaged. Then, the sigma and polarimetric parameters values were extracted and

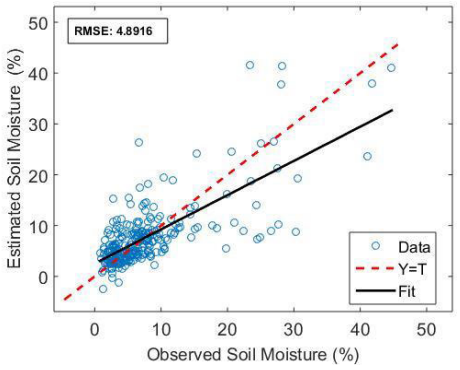

FIGURE 11. Soil moisture inversion using feature vector consists of Yamaguchi decomposition components by means of LS-SVM machine learning method for all samples of 10 June 2015.

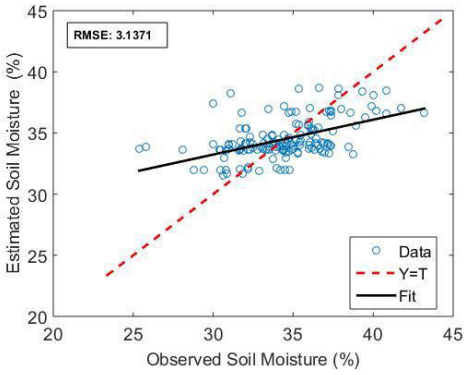

FIGURE 12. Soil moisture inversion using feature vector consists of Yamaguchi decomposition components by means of LS-SVM machine learning method for all samples of 3 March 2016.

these values were recorded to use as an input for semiempirical and machine learning models. The extracted values from Radarsat-2 images for each point of ground measurements were 4 sigma nought values, 4 Yamaguchi decomposition values, 3 van Zyl decomposition values, 3 Freeman-Durden decomposition values, 3 Cloude-Pottier decomposition values, 3 Cloude decomposition values. Eventually, a total of 20 features were generated for each cell. This process was repeated for 272 sampling points of 10 June 2015 and 156 sample points of 3 March 2016 Radarsat-2 images. The parameters extracted from the image for polarimetric decomposition methods were summarized in Table 3. The final Radarsat-2 SAR data derived for two periods using sigma nought and polarimetric techniques were presented in Figure 6 and 7.

Performance measurement for model estimates was performed with root mean square error (RMSE). RMSE is a common tool used to measure the difference between values estimated by a model and the values measured. In this study, this statistical index is expressed as the percentage of volumetric soil moisture. RMSE is calculated with the following formula:

$$RMSE = \sqrt{\frac{1}{N}\sum_{i=1}^{N}(e_i - o_i)^2} \tag{28}$$

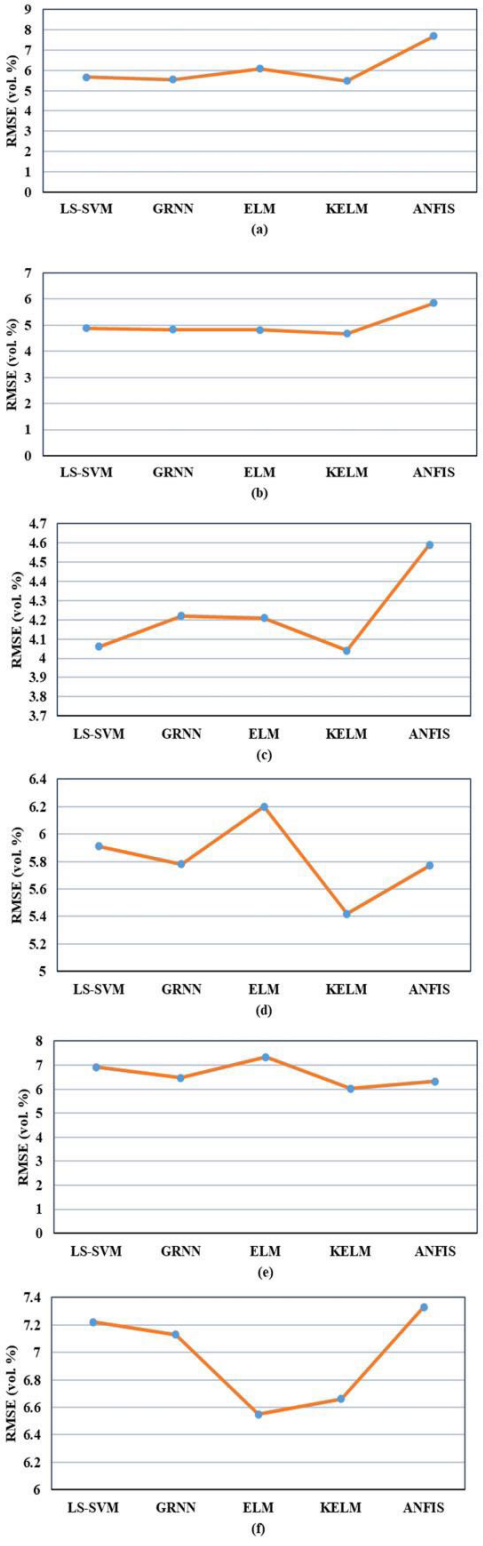

FIGURE 13. RMSE (vol. %) values of soil moisture inversion using machine learning models from 10 June 2015 Radarsat-2 data for feature vector containing (a) Sigma nought values, (b) Yamaguchi decomposition components, (c) Generalized Freeman-Durden decomposition components, (d) van Zyl decomposition components, (e) Cloude decomposition components, (f) H/A/α decomposition components.

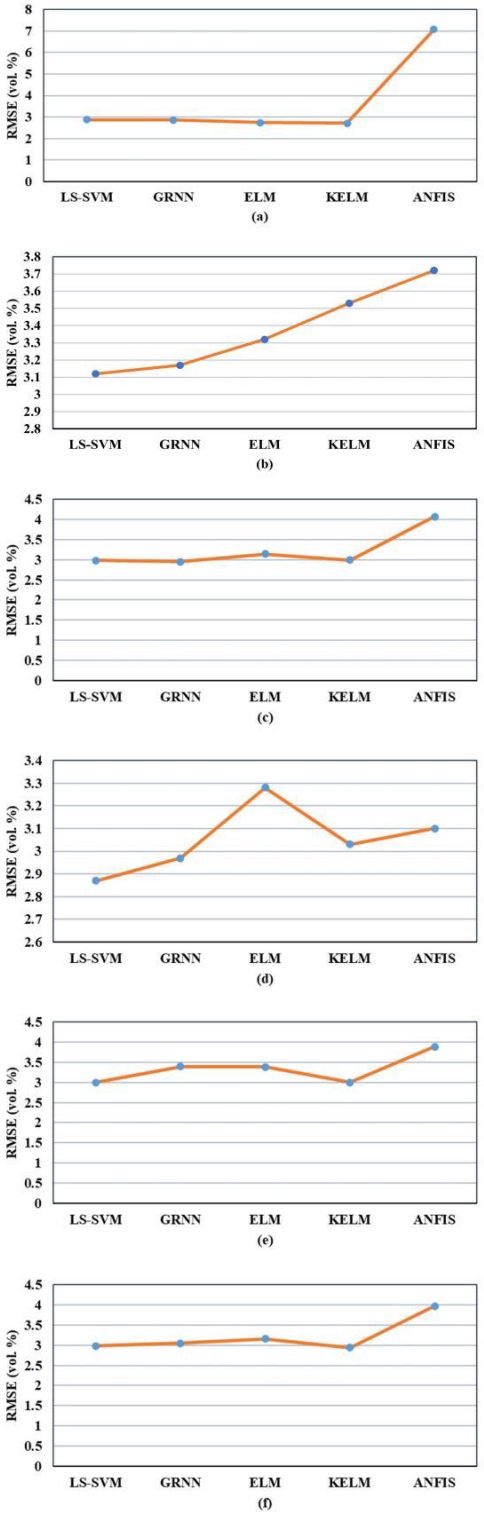

FIGURE 14. RMSE (vol. %) values of soil moisture inversion using machine learning models from 3 March 2016 Radarsat-2 data for feature vector containing (a) Sigma nought values, (b) Yamaguchi decomposition components, (c) Generalized Freeman Durden decomposition components, (d) van Zyl decomposition components, (e) Cloude decomposition components, (f) H/A/α decomposition components.

where N is the number of samples, m_i is the observed value of sample i, and e_i is the estimated value of sample i.

The semiempirical Oh (1992), Dubois (1995) and Oh (2004) were evaluated to retrieve the surface soil

TABLE 4. The comparison of different approaches for soil moisture inversion.

Reference	Province	Dataset	Performance	Methods
Proposed method	Bare and vegetated fields (Turkey)	Radarsat-2 data & Ground Measurements	RMSE = 13.01 % with semiempirical methods, RMSE = 2.72 % with machine learning	Semiempirical methods, Polarimetric decompositions, Machine learning
[33]	Vegetated lands (North America)	CYGNSS data & Ground Measurements	RMSE = 5.12 %	Machine Learning based algorithm
[13]	Bare fields (Europe)	ERS-SAR & Ground Measurements	RMSE = 6 %	ANN
[34]	Vegetated fields (Canada)	UAVSAR & SMAP datasets	RMSE = 6 - 12 %	Polarimetric decomposition
[35]	Bare fields (France)	Radarsat-2 & IEM datasets	RMSE = 6.5 - 9.8 %	ANN
[36]	Vegetated fields (China)	Radarsat-2 data & Ground Measurements	RMSE = 1.76 - 2.81 %	Polarimetric decomposition, Bragg, X-Bragg, ISSM
[4]	Bare fields (China)	TerraSAR-X, Radarsat-2 & Ground Measurements	RMSE = 2.2 - 3 %	SVR, Modified Dubois model
[37]	Bare and vegetated fields (USA)	Landsat, Radarsat-1 & Ground Measurements	RMSE = 3.39 – 8.29 %	Multiple regression, Neural network, Fuzzy logic
[15]	Vegetated fields (Italy)	Radarsat-2 data & Ground Measurements	RMSE = 4.85 %	SVR, Polarimetric decomposition
[38]	Vegetated fields (Canada)	Radarsat-2 data & Ground Measurements	RMSE = 4.43 %	MWCM

moisture content. These semiempirical models are not as complicated as theoretical models but not as simple as empirical models. The semiempirical soil moisture inversions were calculated based on preprocessed imagery by means of PolSARpro source code of these models. The PolSARpro is open-source SAR analysis software created by the European Space Agency (ESA). The source code for the three surface inversion models was evaluated to retrieve dielectric constant and volumetric soil moisture. The Oh (1992) and Dubois (1995) models retrieve the dielectric constant and Oh (2004) model directly retrieves the volumetric soil moisture.

The accuracy of semiempirical models were obtained as 13.01 vol % RMSE for 10 June 2015 sample points using Dubois (1995) model and 22.93 vol % RMSE for 3 March 2016 sample points using Oh (1992). The sample scatter plots given in Figure 8 and 9 show the relationship between the retrieved and observed soil moisture for 10 June 2015 Radarsat-2 data with Dubois (1995) model and 3 March 2016 Radarsat-2 data with Oh (1992) model, respectively. The results of all semiempirical models for two periods are presented in Figure 10.

It is seen that most of the soil moisture inversions carried out with the semiempirical approach for the datasets of 10 June 2015 and 3 March 2016 were out of the validity ranges of models. Soil moisture inversions carried out with Oh (1992), Dubois (1995) and Oh (2004) for 10 June 2015 dataset, 74, 74 and 11 inversions were in the model validity ranges, respectively, and for 3 March 2016 dataset, 54, 106, 16 inversions were in the model validity ranges, respectively.

In the machine learning approach, soil moisture inversion was performed using 5 different methods which were LS-SVM, GRNN, ELM, KELM and ANFIS. Training and test sets were created to calculate the success of these methods. Soil moisture ground measurements were defined as the target vector for machine learning methods. In the testing phase, 10-fold cross-validation was used to validate the success of the system. In k-fold cross-validation method [32], the data set is randomly divided into k parts. Each time, one part of this data set is used for testing while the rest is used for training. At the end of k trials, each part of data is used for testing and the accuracy of the system is calculated as the average of the error obtained for all data parts.

The accuracy of the machine learning models, for example, were obtained 4.80 vol % RMSE for all samples of 10 June 2015 and 3.13 vol % RMSE for 3 March 2016 by using the LS-SVM model. This model was trained with the dataset containing Yamaguchi decomposition coefficients as input. Among the machine learning approaches used, LS-SVM, GRNN, ELM and KELM generally gave the best RMSE results for both periods. The RMSE values obtained with ANFIS were mostly higher. The scatter plots given in Figure 11 and 12 show the relationship between the estimated value by LS-SVM machine learning model using feature vector consist of Yamaguchi decomposition components and measured soil moistures for 10 June 2015 and 3 March 2016, respectively. The calculated RMSE results of all machine learning models using different feature vectors as input are presented in Figure 13 and 14 for 10 June 2015 and 3 March 2016, respectively.

When all results are compared, the inversion of soil moisture with semiempirical models gave much worse results than the machine learning approach. This might be because the surface of study area is covered with vegetation. Moreover, in order to get accurate results from semiempirical models, the parameters, which include soil moisture, radar incidence angle and surface roughness, must be in model validity ranges. Otherwise, the models cannot produce accurate results, and this restricts the use of semiempirical models.

Although the machine learning approach gave better results than semiempirical models for soil moisture inversion, it has some drawbacks. One of the main disadvantages of machine learning approach is that it needs to collect a large number of samples for the acceptable accuracy of results. Looking at the machine learning methods used in this study; GRNN, ELM and KELM methods were much faster than LS-SVM and ANFIS methods during the training of the model.

Several other literature studies on soil moisture inversion by different approaches were given in Table 4. It can be said that the proposed models in this study also produce good and noticeable results compared to the other studies in the literature.

V. CONCLUSION

In this study, the performance of semiempirical and machine learning models was evaluated for soil moisture inversion employing Radarsat-2 SAR imagery.

The results indicated that the machine learning models could perform much better compared to the semi empirical models for soil moisture inversion because semiempirical models only give accurate results depending on the soil moisture, radar incidence angle and surface roughness parameters in model validity ranges. Therefore, this limits the usage area of semiempirical models. When machine-learning methods used in this study are considered, GRNN, ELM and KELM were very fast, however LS-SVM and ANFIS had more computation time in training stage.

To sum up, the results of this study showed that SAR remote sensing data could be used for soil moisture inversion fast and with acceptable accuracy thanks to machine learning approach.

In future studies, it is planned to conduct comprehensive analysis for soil moisture inversion with the combination of active and passive sensor data and more ground truth measurements to improve the proposed approach.

AUTHOR CONTRIBUTIONS

Mehmet Siraç Özerdem designed the research; Mehmet Siraç Özerdem and Emrullah Acar contributed to field measurements; Mehmet Siraç Özerdem contributed to materials and analysis tools; Hüseyin Acar performed the software analysis; Hüseyin Acar, Mehmet Siraç Özerdem and Emrullah Acar analyzed the results and prepared the original paper.

CONFLICTS OF INTEREST

The authors declare no conflict of interest.

ACKNOWLEDGMENT

The authors would like to thank the ESA for providing the SNAP and PolSARpro software.

REFERENCES

[1] M. Xing, B. He, X. Ni, J. Wang, G. An, J. Shang, and X. Huang, "Retrieving surface soil moisture over wheat and soybean fields during growing season using modified water cloud model from Radarsat-2 SAR data," *Remote Sens.*, vol. 11, no. 16, p. 1956, Aug. 2019, doi: 10.3390/rs11161956.

[2] N. Verhoest, H. Lievens, W. Wagner, J. Álvarez-Mozos, M. Moran, and F. Mattia, "On the soil roughness parameterization problem in soil moisture retrieval of bare surfaces from synthetic aperture radar," *Sensors*, vol. 8, no. 7, pp. 4213–4248, Jul. 2008, doi: 10.3390/s8074213.

[3] A. Merzouki, H. McNairn, and A. Pacheco, "Evaluation of the dubois, oh, and IEM radar backscatter models over agricultural fields using C-band RADARSAT-2 SAR image data," *Can. J. Remote Sens.*, vol. 36, no. sup2, pp. S274–S286, Jan. 2010, doi: 10.5589/m10-055.

[4] X. Zhang, B. Chen, H. Fan, J. Huang, and H. Zhao, "The potential use of multi-band SAR data for soil moisture retrieval over bare agricultural areas: Hebei, China," *Remote Sens.*, vol. 8, no. 1, pp. 1–14, 2016, doi: 10.3390/rs8010007.

[5] B. Deschamps, "Evaluation of three semi-empirical soil moisture estimation models with RADARSAT-2 imagery," M.S. thesis, Dept. Graduate Stud. Res., Carleton Univ., Ottawa, ON, Canada, 2010.

[6] C. Oliver and S. Quegan, *Understanding Synthetic Aperture Radar Images*. Stevenage, U.K.: SciTech, 2004.

[7] B. He, M. Xing, and X. Bai, "A synergistic methodology for soil moisture estimation in an alpine prairie using radar and optical satellite data," *Remote Sens.*, vol. 6, no. 11, pp. 10966–10985, Nov. 2014, doi: 10.3390/rs61110966.

[8] Y. Oh, K. Sarabandi, and F. T. Ulaby, "An empirical model and an inversion technique for radar scattering from bare soil surfaces," *IEEE Trans. Geosci. Remote Sens.*, vol. 30, no. 2, pp. 370–381, Mar. 1992, doi: 10.1109/36.134086.

[9] P. C. Dubois, J. van Zyl, and T. Engman, "Measuring soil moisture with imaging radars," *IEEE Trans. Geosci. Remote Sens.*, vol. 33, no. 4, pp. 915–926, Jul. 1995, doi: 10.1109/36.406677.

[10] Y. Oh, "Quantitative retrieval of soil moisture content and surface roughness from multipolarized radar observations of bare soil surfaces," *IEEE Trans. Geosci. Remote Sens.*, vol. 42, no. 3, pp. 596–601, Mar. 2004, doi: 10.1109/TGRS.2003.821065.

[11] A. K. Fung, Z. Li, and K. S. Chen, "Backscattering from a randomly rough dielectric surface," *IEEE Trans. Geosci. Remote Sens.*, vol. 30, no. 2, pp. 356–369, Mar. 1992, doi: 10.1109/36.134085.

[12] I. Ali, F. Greifeneder, J. Stamenkovic, M. Neumann, and C. Notarnicola, "Review of machine learning approaches for biomass and soil moisture retrievals from remote sensing data," *Remote Sens.*, vol. 7, no. 12, pp. 16398–16421, Dec. 2015, doi: 10.3390/rs71215841.

[13] G. Satalino, F. Mattia, M. W. J. Davidson, T. Le Toan, G. Pasquariello, and M. Borgeaud, "On current limits of soil moisture retrieval from ERS-SAR data," *IEEE Trans. Geosci. Remote Sens.*, vol. 40, no. 11, pp. 2438–2447, Nov. 2002, doi: 10.1109/TGRS.2002.803790.

[14] S. Paloscia, S. Pettinato, E. Santi, C. Notarnicola, L. Pasolli, and A. Reppucci, "Soil moisture mapping using Sentinel-1 images: Algorithm and preliminary validation," *Remote Sens. Environ.*, vol. 134, pp. 234–248, Jul. 2013, doi: 10.1016/j.rse.2013.02.027.

[15] L. Pasolli, C. Notarnicola, L. Bruzzone, G. Bertoldi, S. D. Chiesa, G. Niedrist, U. Tappeiner, and M. Zebisch, "Polarimetric RADARSAT-2 imagery for soil moisture retrieval in alpine areas," *Can. J. Remote Sens.*, vol. 37, no. 5, pp. 535–547, Oct. 2011, doi: 10.5589/m11-065.

[16] M. S. Özerdem, E. Acar, and R. Ekinci, "Soil moisture estimation over vegetated agricultural areas: Tigris basin, turkey from Radarsat-2 data by polarimetric decomposition models and a generalized regression neural network," *Remote Sens.*, vol. 9, no. 4, p. 395, Apr. 2017, doi: 10.3390/rs9040395.

[17] G. C. Topp, J. L. Davis, and A. P. Annan, "Electromagnetic determination of soil water content: Measurements in coaxial transmission lines," *Water Resour. Res.*, vol. 16, no. 3, pp. 574–582, Jun. 1980, doi: 10.1029/WR016i003p00574.

[18] Y. Oh, K. Sarabandi, and F. T. Ulaby, "Semi-empirical model of the ensemble-averaged differential mueller matrix for microwave backscattering from bare soil surfaces," *IEEE Trans. Geosci. Remote Sens.*, vol. 40, no. 6, pp. 1348–1355, Jun. 2002, doi: 10.1109/TGRS.2002.800232.

[19] Y. Oh and Y. Chul Kay, "Condition for precise measurement of soil surface roughness," *IEEE Trans. Geosci. Remote Sens.*, vol. 36, no. 2, pp. 691–695, Mar. 1998, doi: 10.1109/36.662751.

[20] V. N. Vapnik, *The Nature of Statistical Learning Theory*. Berlin, Germany: Springer-Verlag, 1995.

[21] N. Ceryan, U. Okkan, P. Samui, and S. Ceryan, "Modeling of tensile strength of rocks materials based on support vector machines approaches," *Int. J. Numer. Anal. Methods Geomechanics*, vol. 37, no. 16, pp. 2655–2670, Nov. 2013.

[22] J. Suykens and J. Van Gestel, "De Brabanter, B. De Moor, and J. Vandewalle, "Least squares support vector machines," *Neurocomputing*, vol. 48, pp. 85–105, Oct. 2002.

[23] J. A. K. Suykens, J. Vandewalle, and B. De Moor, "Optimal control by least squares support vector machines," *Neural Netw.*, vol. 14, pp. 23–35, Jan. 2001, doi: 10.1016/S0893-6080(00)00077-0.

[24] D. F. Specht, "A general regression neural network," *IEEE Trans. Neural Netw.*, vol. 2, no. 6, pp. 568–576, Nov. 1991, doi: 10.1109/72.97934.

[25] G.-B. Huang, Q.-Y. Zhu, and C.-K. Siew, "Extreme learning machine: Theory and applications," *Neurocomputing*, vol. 70, nos. 1–3, pp. 489–501, Dec. 2006, doi: 10.1016/j.neucom.2005.12.126.

[26] J.-S.-R. Jang, "ANFIS: Adaptive-network-based fuzzy inference system," *IEEE Trans. Syst., Man, Cybern.*, vol. 23, no. 3, pp. 665–685, May 1993, doi: 10.1109/21.256541.

[27] K. Dasari, A. Lokam, and P. V. Jayasri, "A study on utilization of polarimetric SAR data in planning a smart city," *Procedia Comput. Sci.*, vol. 93, pp. 967–974, 2016, doi: 10.1016/j.procs.2016.07.287.

[28] Y. Yamaguchi, T. Moriyama, M. Ishido, and H. Yamada, "Four-component scattering model for polarimetric SAR image decomposition," *IEEE Trans. Geosci. Remote Sens.*, vol. 43, no. 8, pp. 1699–1706, Aug. 2005, doi: 10.1109/TGRS.2005.852084.

[29] J. J. van Zyl, M. Arii, and Y. Kim, "Model-based decomposition of polarimetric SAR covariance matrices constrained for nonnegative eigenvalues," *IEEE Trans. Geosci. Remote Sens.*, vol. 49, no. 9, pp. 3452–3459, Sep. 2011, doi: 10.1109/TGRS.2011.2128325.

[30] J.-S. Lee and E. Pottier, *Polarimetric Radar Imaging: From Basics to Applications*. Boca Raton, FL, USA: CRC Press, 2017.

[31] M. Ustuner and F. Balik Sanli, "Polarimetric target decompositions and light gradient boosting machine for crop classification: A comparative evaluation," *ISPRS Int. J. Geo-Inf.*, vol. 8, no. 2, p. 97, Feb. 2019, doi: 10.3390/ijgi8020097.

[32] A. Sengur, "Multiclass least-squares support vector machines for analog modulation classification," *Expert Syst. Appl.*, vol. 36, no. 3, pp. 6681–6685, Apr. 2009, doi: 10.1016/j.eswa.2008.08.066.

[33] V. Senyurek, F. Lei, D. Boyd, M. Kurum, A. C. Gurbuz, and R. Moorhead, "Machine learning-based CYGNSS soil moisture estimates over ISMN sites in CONUS," *Remote Sens.*, vol. 12, no. 7, pp. 1–24, 2020, doi: 10.3390/rs12071168.

[34] H. Wang, R. Magagi, K. Goita, T. Jagdhuber, and I. Hajnsek, "Evaluation of simplified polarimetric decomposition for soil moisture retrieval over vegetated agricultural fields," *Remote Sens.*, vol. 8, no. 2, pp. 1–24, 2016, doi: 10.3390/rs8020142.

[35] N. Baghdadi, R. Cresson, M. El Hajj, R. Ludwig, and I. La Jeunesse, "Estimation of soil parameters over bare agriculture areas from C-band polarimetric SAR data using neural networks," *Hydrol. Earth Syst. Sci.*, vol. 16, no. 6, pp. 1607–1621, Jun. 2012, doi: 10.5194/hess-16-1607-2012.

[36] Q. Xie, Q. Meng, L. Zhang, C. Wang, Y. Sun, and Z. Sun, "A soil moisture retrieval method based on typical polarization decomposition techniques for a maize field from full-polarization Radarsat-2 data," *Remote Sens.*, vol. 9, no. 2, p. 168, Feb. 2017, doi: 10.3390/rs9020168.

[37] T. Lakhankar, H. Ghedira, M. Temimi, M. Sengupta, R. Khanbilvardi, and R. Blake, "Non-parametric methods for soil moisture retrieval from satellite remote sensing data," *Remote Sens.*, vol. 1, no. 1, pp. 3–21, Mar. 2009, doi: 10.3390/rs1010003.

[38] M. Xing, B. He, X. Ni, J. Wang, G. An, J. Shang, and X. Huang, "Retrieving surface soil moisture over wheat and soybean fields during growing season using modified water cloud model from Radarsat-2 SAR data," *Remote Sens.*, vol. 11, no. 16, p. 1956, Aug. 2019, doi: 10.3390/rs11161956.

HÜSEYİN ACAR (Member, IEEE) received the B.S. degree in electronics engineering from Uludağ University, Bursa, Turkey, in 2006, and the M.S. degree in electrical and electronics engineering from Dicle University, Diyarbakır, Turkey, in 2010, where he is currently pursuing the Ph.D. degree.

He is currently a Research Assistant with the Electrical and Electronics Engineering Department, Dicle University. His research interests include remote sensing, image processing, and embedded systems.

MEHMET SİRAÇ ÖZERDEM received the B.Sc. degree in electrical–electronics engineering from Eastern Mediterranean University, Northern Cyprus, in 1994, the M.Sc. degree in electrical engineering from Yıldız Technical University, in 1998, and the Ph.D. degree in computer engineering from Istanbul Technical University, in 2003. He is currently a Professor and a Researcher with Dicle University, Diyarbakır, Turkey. His research interests include machine learning, biomedical signal processing, bioinformatics, and embedded system design.

EMRULLAH ACAR received the B.S. degree in electrical and electronics engineering from Çukurova University, Adana, Turkey, in 2009, the M.S. degree in biomedical engineering from Istanbul Technical University, Istanbul, Turkey, in 2010, and the M.S. and Ph.D. degrees in electrical–electronics engineering from Dicle University, Diyarbakır, Turkey, in 2012 and 2017, respectively.

From 2008 to 2009, he was an Exchange Student in electrical engineering from Linköping University, Sweden. He is currently an Assistant Professor of electrical–electronics engineering with Batman University and also the Head of the Electronics Division. His research interests include digital image processing, machine learning, and remote sensing applications.

Dr. Acar received awards and honors include The Scientific and Technological Research Council of Turkey (TUBITAK) Grant, Erasmus Mobility Grant, Sweden, and Erasmus Internship Grant, Germany.